Indian Journal of Chemistry
Vol. 58A, December 2019, pp. 1319-1337

Preparation, structural characterization, antimicrobial and anticancer activities, DFT and molecular docking studies of a nano ferrocenyl Schiff base and its metal complexes

Walaa H Mahmoud[a,b], Reem G Deghadi[a,]* & Gehad G Mohamed[a,b]

[a]Chemistry Department, Faculty of Science, Cairo University, Giza, 12613, Egypt
[b]Egypt Nanotechnology Center, Cairo University, 6th October City, Giza, El-Sheikh Zayed, 12588, Egypt
Email: reemgd90@yahoo.com

Received 27 April 2019; revised and accepted 22 November 2019

An organometallic Schiff base (2-(1-((4-aminopyridin-3-yl)imino)ethyl)cyclopenta-2,4-dien-1-yl) (cyclopenta-2,4-dien-1-yl)iron (L) and eight transition metal complexes have been prepared by reacting 3,4-diaminopyridine with 2-acetylferrocene in 1:1 molar ratio for ligand formation and by reacting Cr(III), Mn(II), Fe(III), Co(II), Ni(II), Cu(II), Zn(II) and Cd(II) chlorides with ligand in 1:1 molar ratio for complexes formation. All prepared compounds have been characterized by using elemental analysis (C, H, N, M), molar conductance, IR, UV-Vis, ^{1}H-NMR, SEM and mass spectral analysis. Also, their TG and DTG behaviors have been studied. All complexes have an octahedral structure. The ligand coordinated to the metal ions through the nitrogen atoms of azomethine and amino groups. In addition, computational studies of the synthesized Schiff base ligand have been carried out by the DFT/B3LYP method. The antimicrobial activities of the ligand and its metal complexes have been studied by using different bacterial species [*Bacillus subtilis*, *Staphylococcus aureus*, *Escherichia coli*, *Salmonella typhimurium*] and fungal species included [*Aspergillus fumigatus* and *Candida albicans*]. Moreover, the prepared compounds have been evaluated for anticancer activities against breast cancer (MCF-7) and normal melanocytes (HFB-4) cell lines. Docking studies have been used to determine the probable binding mode between the ligand and its Cd(II) complex with the active site of 3HB5, 2HQ6 and 1GS4 receptors.

Key words: Organometallic Schiff base, DFT/B3LYP, Biological activity, MCF-7, Docking studies

Schiff bases are considered as a large group of chemical compounds that have an azomethine group (C=N) in their composition. These Schiff bases can be used as antifungal, antibacterial and antimutagenic agents[1,2]. Also, they have comutagenic and DNA interaction properties[3]. The chelation of Schiff bases with different transition metal ions has been investigated to improve the biological potential of these Schiff bases. Hence, metal complexes of various Schiff bases are important to be synthesized[4].

Metallocenes are organometallic compounds that contain a metal ion between two planar polyhapto rings[5]. So, they are called sandwich compounds. One of the most important ligands encountered in metallocenes is cyclopentadienyl (CP). This CP ligand has a very vital role in the development of organometallic chemistry and may be considered as the most common organometallic compound that has been utilized in various areas of chemistry and technology[6].

Synthesis of organometallic ferrocene complexes is very important in organometallic chemistry due to the flexibility, the ease of functionalization of the cyclopentadienyl rings and the redox couple property of Fe(II)/Fe(III)[7]. Ferrocenyl group has a special affinity towards proteins, amino acids, DNA and carbohydrates. So, this group can be widely applied in medicinal designs and biological researches. The organometallic ferrocene drugs have vital pharmacological functions due to the effect of cytotoxicity, lipophilicity and redox property of the ferrocene moiety on biological targets[8–10]. Furthermore, ferrocene-based ligands have been used in various fields such as biosensors, semiconductors, nonlinear optics and asymmetric catalysis[11,12].

In the light of these facts, this article was interested in preparing a novel organometallic Schiff base ligand by condensation of 3,4-diaminopyridine and 2-acetylferrocene. Then its coordination behavior with different transition metal ions was studied. The novel prepared ligand and its metal complexes were characterized using different techniques. Also, their antimicrobial and anticancer activities were investigated. Molecular docking was used to

determine the probable binding mode between the ligand and its Cd(II) complex with the active site of the receptors of breast cancer mutant oxidoreductase (PDB ID: 3HB5), Colon Cancer Antigen 10 from Homo Sapiens (PDB ID: 2HQ6) and mutant human androgen (ARccr) derived from an androgen-independent prostate cancer (PDB ID: 1GS4).

Experimental

Materials and reagents

All chemicals used were of the highest purity and analytical reagent grade (AR). The chemicals used included 2-acetylferrocene which was supplied from Sigma-Aldrich, 3,4-diaminopyridine (Sigma-Aldrich), $CrCl_3.6H_2O$, $MnCl_2.2H_2O$ and $FeCl_3.6H_2O$ (Sigma-Aldrich), $NiCl_2.6H_2O$, $CoCl_2.6H_2O$, $CuCl_2.2H_2O$ and $ZnCl_2$ (BDH) and $CdCl_2$ (Merck). Organic solvents used were ethyl alcohol (95 %), methyl alcohol and *N*,*N*-dimethylformamide (DMF). Deionized water was usually used in all preparations.

Solutions

Stock solutions of the ferrocene Schiff base ligand and its metal complexes of 1×10^{-3} M were prepared by dissolving an accurately weighed amount in *N*,*N*-dimethylformamide for Cr(III), Fe(III), Ni(II) and Cu(II) complexes, in ethanol for Mn(II), Co(II), Zn(II) and Cd(II) complexes and methanol for the Schiff base ligand. The conductivity then measured for the 1×10^{-3} M solution of metal complexes. Dilute solutions of the Schiff base ligand and its metal complexes (1×10^{-4} M) were prepared by accurate dilution from the previously prepared stock solutions for measuring their UV–Vis spectra.

Solution of anticancer study

A fresh stock solution (1×10^{-3} M) of Schiff base ligand (0.12×10^{-2} g L^{-1}) was prepared in the appropriate volume of ethanol (90%). DMSO was used in cryopreservation of cells. RPMI-1640 medium was used. The medium was used for culturing and maintenance of the human tumor cell line. The medium was supplied in a powder form. It was prepared as follows: 10.40 g of a medium was weighed, mixed with 2 g of sodium bicarbonate, completed to 1 L with distilled water and shaken carefully until complete dissolution. The medium was then sterilized by filtration in a Millipore bacterial filter (0.22 mL). The prepared medium was kept in a refrigerator (4 °C) and checked at regular intervals for contamination. The medium was warmed at 37 °C in a water bath before use and supplemented with penicillin-streptomycin, and FBS. Sodium bicarbonate was used for the preparation of RPMI-1640 medium. Isotonic trypan blue solution (0.05%) was prepared in normal saline and was used for viability counting. FBS (10%, heat inactivated at 56 °C for 30 min), 100 units/mL penicillin and 2 mg/mL streptomycin were used for the supplementation of RPMI-1640 medium prior to use. Trypsin (0.25×10^{-1} % w/v) was used for the harvesting of cells. Acetic acid (1% v/v) was used for dissolving unbound SRB dye. SRB (0.40 %) dissolved in 1% acetic acid was used as a protein dye. A stock solution of trichloroacetic acid (50%) was prepared and stored. An amount of 50 µL of the stock was added to 200 µL of RPMI-1640 medium per well to yield a final concentration of 10% used for protein precipitation. Isopropanol (100%) and ethanol (70%) were used. Tris base (10 mM; pH = 10.50) was used for SRB dye solubilization. Tris base (121.10 g) was dissolved in 1000 mL of distilled water and the pH was adjusted using hydrochloric acid (2 M).

Instrumentation

Microanalyses of carbon, nitrogen, and hydrogen were carried out at the Microanalytical Center, Cairo University, Egypt, using a CHNS-932 (LECO) Vario elemental analyzer. Analyses of the metals were conducted by dissolving the solid complexes in concentrated HNO_3 and dissolving the residue in deionized water. The metal content was carried out using inductively coupled plasma atomic absorption spectrometry (ICP-AES), Egyptian Petroleum Research Institute. Fourier transform infrared (FT-IR) spectra were recorded with a PerkinElmer 1650 spectrometer (400–4000 cm^{-1}) as KBr pellets. ^{1}H-NMR spectra, as solutions in DMSO-d_6, were recorded with a 300 MHz Varian-Oxford Mercury at room temperature using tetramethylsilane as an internal standard. Mass spectra were recorded using the electron ionization technique at 70 eV with an MS-5988 GS-MS Hewlett-Packard instrument at the Microanalytical Center, National Center for Research, Egypt. UV–Visible spectra were obtained with a Shimadzu UVmini-1240 spectrophotometer. Molar conductivities of 1×10^{-3} M solutions of the solid complexes were measured using a Jenway 4010 conductivity meter. Thermogravimetric (TG) and differential thermogravimetric (DTG) analyses of the solid complexes were carried out from room temperature to 1000 °C using a Shimadzu TG-50H

thermal analyzer. Antimicrobial measurements were carried out at the Microanalytical Center, Cairo University, Egypt. Anticancer activity experiments were performed at the National Cancer Institute, Cancer Biology Department, Pharmacology Department, Cairo University. The optical density (OD) of each well was measured spectrophotometrically at 564 nm with an ELIZA microplate reader (Meter tech. R960, USA). The scanning electron microscope (SEM) image of the complexes was recorded by using SEM Model Quanta 250 FEG (Field Emission Gun) attached with EDX unit (Energy Dispersive X-ray Analyses), with accelerating voltage 30 K V, magnification 14X up to 1000000 and resolution for Gun.1n, National Research Center, Egypt).

Synthesis of organometallic Schiff base ligand (L)

The organometallic Schiff base ligand (L) was prepared by refluxing a hot mixture of 3,4-diaminopyridine (0.03 mol, 3.27 g) dissolved in ethanol and 2-acetylferrocene (0.03 mol, 7 g) dissolved in methanol. The resulting mixture was stirred under reflux for about 2 h, during which a brown solid compound was separated. It was filtered, recrystallized, washed with diethyl ether and dried in vacuum. Preparation of organometallic Schiff base (L) as shown in Scheme 1.

(2-(1-((4-aminopyridin-3-yl)imino)ethyl)cyclopenta-2,4-dien-1-yl) (cyclopenta-2,4-dien-1-yl)iron (L). Yield 98%; M.P.: 100 °C; brown solid. Anal. Calcd. for $C_{17}H_{17}FeN_3$ (%): C, 63.95; H, 5.33; N, 13.17; Fe, 17.56. Found (%): C, 63.71; H, 5.09; N, 13.08; Fe, 17.18. FT-IR (ν, cm^{-1}): azomethine (C=N) 1659sh, N-pyridine ring 1108m, amino group $(NH_2)_{bending}$ 616w. ^1H NMR (300 MHz, DMSO-d_6, δ, ppm): 4.23–4.77 (m, 9H, ferrocene ring), 6.56–7.69 (m, 3H, aromatic ring), 5.29 (s, 2H, amino group), 1.26 (s, 3H, methyl group). UV-Vis (λ_{max}, nm): 230, 273 (π–π* of ferrocene and benzene rings) and 306 (π–π* of azomethine).

Synthesis of metal complexes

The Cr(III), Mn(II), Fe(III), Co(II), Ni(II), Cu(II), Zn(II) and Cd(II) complexes were prepared by a reaction of 1:1 molar mixture of hot ethanolic solution (60 °C) of the metal chloride (1.25×10^{-3} mol) and the methanolic solution of Schiff base ligand (L) (0.4 g, 1.25×10^{-3} mol). The formed mixture was stirred under reflux for 1 h, whereupon the complexes precipitated. They were collected by filtration and purified by washing several times with diethyl ether. The solid complexes then dried in a desiccator over anhydrous calcium chloride.

$[Cr(L)(H_2O)_2Cl_2]Cl.2H_2O$

Yield 91%; M.P.: >300 °C; dark brown solid. Anal. Calcd. for $C_{17}H_{25}Cl_3FeCrN_3O_4$ (%): C, 37.13; H, 4.55; N, 7.64; Fe, 10.19; Cr, 9.46. Found (%): C, 37.05; H, 4.32; N, 7.29; Fe, 10.02; Cr, 9.25. Λ_m (Ω^{-1} mol^{-1} cm^2) = 65; FT-IR (ν, cm^{-1}): azomethine (C=N) 1638m, H_2O stretching of coordinated water 878w and 800w, amino group $(NH_2)_{bending}$ 608w, (M─O coordinated water) 551s, (M─N) 500w. UV-Vis (λ_{max}, nm): 265 (π–π*).

$[Mn(L)(H_2O)_3Cl]Cl.2H_2O$

Yield 88%; M.P.: 150 °C; brown solid. Anal. Calcd. for $C_{17}H_{27}Cl_2FeMnN_3O_5$ (%): C, 38.13; H, 5.05; N, 7.85; Fe, 10.47; Mn, 10.28. Found (%): C, 38.08; H, 5.04; N, 7.61; Fe, 10.23; Mn, 10.11. Λ_m (Ω^{-1} mol^{-1} cm^2) = 72; FT-IR (ν, cm^{-1}): azomethine (C=N) 1655sh, H_2O stretching of coordinated water 890s and 825m, amino group $(NH_2)_{bending}$ 618m, (M─O coordinated water) 531s, (M─N) 499s. UV-Vis (λ_{max}, nm): 231 (π–π* of ferrocene and benzene rings) and 301 (π–π* of azomethine).

$[Fe(L)(H_2O)Cl_3].5H_2O$

Yield 79%; M.P.: >300 °C; dark brown solid. Anal. Calcd. for $C_{17}H_{29}Cl_3Fe_2N_3O_6$ (%): C, 34.61; H, 4.92; N, 7.13; Fe, 18.68. Found (%): C, 34.24; H, 4.72; N, 7.02; Fe, 19.68. Λ_m (Ω^{-1} mol^{-1} cm^2) = 40; FT-IR (ν, cm^{-1}): azomethine (C=N) 1642m, H_2O stretching of coordinated water 880w and 802s, amino group

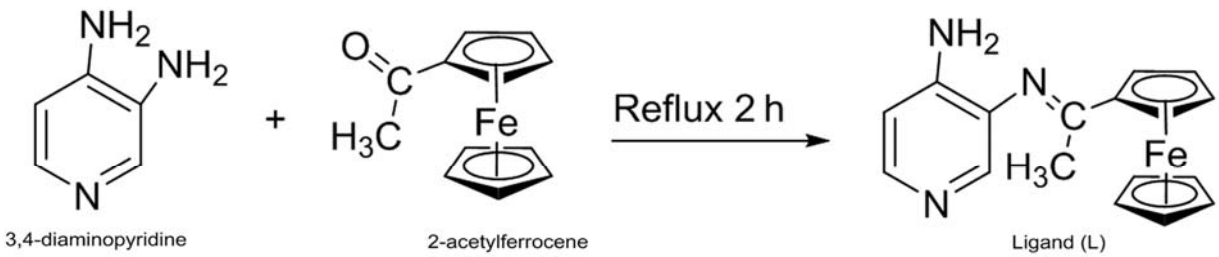

Preparation of organometallic Schiff base (L)
Scheme 1

$(NH_2)_{bending}$ 681s, (M─O coordinated water) 580w, (M─N) 480w. UV-Vis (λ_{max}, nm): 263 (π –π*).

[Co(L)$(H_2O)_3$Cl]Cl.H_2O

Yield 85%; M.P.: 90 °C; brown solid. Anal. Calcd. for $C_{17}H_{25}Cl_2FeCoN_3O_4$ (%): C, 39.16; H, 4.80; N, 8.06; Fe, 10.75; Co, 11.32. Found (%): C, 39.03; H, 4.45; N, 8.01; Fe, 10.34; Co, 11.22. Λ_m (Ω^{-1} mol^{-1} cm^2) = 75; FT-IR (ν, cm^{-1}): azomethine (C=N) 1655sh, H_2O stretching of coordinated water 887w and 817m, amino group $(NH_2)_{bending}$ 618m, (M─O coordinated water) 532s, (M─N) 489s. UV-Vis (λ_{max}, nm): 231 (π–π* of ferrocene and benzene rings) and 302 (π–π* of azomethine).

[Ni(L)$(H_2O)_3$Cl]Cl.H_2O

Yield 90%; M.P.: >300 °C; dark brown solid. Anal. Calcd. for $C_{17}H_{25}Cl_2FeNiN_3O_4$ (%): C, 39.16; H, 4.80; N, 8.06; Fe, 10.75; Ni, 11.32. Found (%): C, 39.03; H, 4.47; N, 8.02; Fe, 10.43; Ni, 11.14. Λ_m (Ω^{-1} mol^{-1} cm^2) = 73; FT-IR (ν, cm^{-1}): azomethine (C=N) 1643m, H_2O stretching of coordinated water 980w and 877w, amino group $(NH_2)_{bending}$ 660w, (M─O coordinated water) 529w, (M─N) 480w. UV-Vis (λ_{max}, nm): 231, 297 (π–π*).

[Cu(L)$(H_2O)_2Cl_2$].$2H_2O$

Yield 78%; M.P.: >300 °C; dark brown solid. Anal. Calcd. for $C_{17}H_{25}Cl_2FeCuN_3O_4$ (%): C, 38.82; H, 4.76; N, 7.99; Fe, 10.66; Cu, 11.03. Found (%): C, 38.62; H, 4.58; N, 7.55; Fe, 10.32; Cu, 11.49. Λ_m (Ω^{-1} mol^{-1} cm^2) = 37; FT-IR (ν, cm^{-1}): azomethine (C=N) 1644sh, H_2O stretching of coordinated water 889w and 818w, amino group $(NH_2)_{bending}$ 640w, (M─O coordinated water) 531w, (M─N) 495w. UV-Vis (λ_{max}, nm): 265 (π–π*).

[Zn(L)$(H_2O)_2Cl_2$]

Yield 89%; M.P.: 225 °C; brown solid. Anal. Calcd. for $C_{17}H_{21}FeZnN_3O_2$ (%): C, 41.55; H, 4.28; N, 8.55; Fe, 11.41; Zn, 13.24. Found (%): C, 41.40; H, 4.18; N, 8.38; Fe, 11.32; Zn, 13.08. Λ_m (Ω^{-1} mol^{-1} cm^2) = 29; FT-IR (ν, cm^{-1}): azomethine (C=N) 1649sh, H_2O stretching of coordinated water 897s and 827m, amino group $(NH_2)_{bending}$ 619w, (M─O coordinated water) 533w, (M─N) 488s. UV-Vis (λ_{max}, nm): 231, 275 (π–π* of ferrocene and benzene rings) and 300 (π–π* of azomethine). ^{1}H NMR (300 MHz, DMSO-d_6, δ, ppm): 4.20–4.75 (m, 9H, ferrocene ring), 6.26–7.58 (m, 3H, aromatic ring), 4.96 (s, 2H, amino group), 1.20 (s, 3H, methyl group).

[Cd(L)$(H_2O)_2Cl_2$].$5H_2O$

Yield 90%; M.P.: 225 °C; brown solid. Anal. Calcd. for $C_{17}H_{31}Cl_2FeCdN_3O_7$ (%): C, 32.48; H, 4.94; N, 6.69; Fe, 8.92; Cd, 17.83. Found (%): C, 32.04; H, 4.47; N, 6.28; Fe, 8.47; Cd, 17.38. Λ_m (Ω^{-1} mol^{-1} cm^2) = 16; FT-IR (ν, cm^{-1}): azomethine (C=N) 1649sh, H_2O stretching of coordinated water 885w and 823m, amino group $(NH_2)_{bending}$ 618sh, (M─O coordinated water) 532w, (M─N) 490s. UV-Vis (λ_{max}, nm): 231, 276 (π–π*).

Spectrophotometric studies

The absorption spectra were recorded for 1×10^{-4} M solutions of the free organometallic Schiff base and its metal complexes. The spectra were scanned within the wavelength range from 200 to 700 nm.

Antimicrobial activity

The *in vitro* antibacterial and antifungal activity tests were performed through the disc diffusion method[13]. The bacterial organisms that have been used were *Bacillus subtilis*, *Staphylococcus aureus*, *Escherichia coli,* and *Salmonella typhimurium* and fungal species included *Aspergillus fumigatus* and *Candida albicans*. Stock solution (0.001 mol) was prepared by dissolving the ligand and its complexes in DMSO. The nutrient agar medium for antibacterial was (0.5% Peptone, 0.1% Beef extract, 0.2% Yeast extract, 0.5% NaCl and 1.5% Agar-Agar) was prepared, cooled to 47 °C and then seeded with tested microorganisms. After solidification, 5 mm diameter holes were punched by a sterile corkborer. The investigated compounds, i.e. Schiff base ligand and its metal complexes, were introduced in Petri-dishes (only 0.1 m) after dissolving in DMSO at 1.0×10^{-3} M. These culture plates were then incubated at 37 °C for 20 h for bacteria. By measuring the diameter of the inhibition zone (in mm), the activity can be determined. The plates were kept for incubation at 37 °C for 24 h and then the plates were examined for the formation of the zone of inhibition. The diameter of the inhibition zone was measured in millimeters. Antimicrobial activities were performed in triplicate and the average was taken as the final reading[14].

Anticancer activity

Potential cytotoxicity of all prepared compounds was tested using the method of Skehan and Storeng[15]. Cells were plated in 96-multiwell plate (104 cells/well) for 24 h before treatment with the compounds to allow attachment of the cell to the wall of the plate. Different concentrations of the compounds under investigation (0, 5, 12.5, 25, 50 and 100 µg/mL) were added to the cell monolayer and triplicate wells were prepared for

each individual dose. The monolayer cells were incubated with the compounds for 48 h at 37 °C and in 5% CO_2 atmosphere. Cells were fixed, washed and then stained with SRB stain after 48 h. Removing the excess stain by washing with acetic acid and the attached stain was recovered with tris-EDTA buffer. The optical density (O.D.) of each well was measured spectrophotometrically at 564 nm with an ELIZA microplate reader and the mean background absorbance was automatically subtracted and mean values of each drug concentration was calculated. The relation between drug concentration and the surviving fraction is plotted to get the survival curve of breast tumor cell line for each compound.

Calculation:

The percentage of cell survival was determined by following equation:

Survival fraction = O.D. (treated cells) / O.D. (control cells)

The IC_{50} values (the concentrations of the Schiff base ligand (L) or complexes required to produce 50% inhibition of cell growth). This experiment was repeated 3 times.

Computational methodology

DFT and molecular modelling theoretical calculations for organometallic Schiff base ligand (L) were carried out on Gaussian03 package, at DFT (Density functional theory) level of theory. The molecular geometry for the tested ligand was fully optimized using density functional theory based on the B3LYP method along with the LANL2DZ basis set[16]. The optimized structure of the ligand (L) was visualized using Chemcraft version 1.6 package[17], and GaussView version 5.0.9[18]. Quantum chemical parameters such as the highest occupied molecular orbital energy (E_{HOMO}), the lowest unoccupied molecular orbital energy (E_{LUMO}) and HOMO–LUMO energy gap (ΔE) for the investigated molecule were calculated.

Molecular docking

Molecular docking studies were elaborated using MOE 2008 software and it is a rigid molecular docking software. These studies are very important for predicting the possible binding modes of the most active compounds against the receptors of breast cancer mutant oxidoreductase (PDB ID: 3HB5), Colon Cancer Antigen 10 from *Homo sapiens* (PDB ID: 2HQ6) and a mutant human androgen receptor (ARccr) derived from an androgen-independent prostate cancer (PDB ID: 1GS4)[19]. Docking is an interactive molecular graphics program can be used to calculate and display feasible docking modes of a receptor and ligand and complex molecules. It necessitates the ligand, the receptor as input in PDB format. The water molecules, co-crystallized ligands and other unsupported elements (e.g., Na, K, Hg, etc.,) were removed but the amino acid chain was kept[20]. The structure of ligand in PDB file format was created by Gaussian03 software. The crystal structures of the three receptors were downloaded from the protein data bank (http://www.rcsb.org./pdb).

Results and Discussion

Characterization of organometallic Schiff base ligand (L)

A novel organometallic Schiff base (L) was prepared by condensation of 3,4-diaminopyridine with 2-acetylferrocene. Its structure was characterized based on elemental analysis, IR, mass, ^{1}H-NMR, and SEM. From the mass spectrum of the ligand (L), it showed a peak at 318.75 amu which corresponds to the molecular ion (m/z) peak. This data confirmed the proposed formula in which the ligand moiety was $C_{17}H_{17}FeN_3$ with atomic mass 319 g/mol. Proposed fragmentation pattern for the ligand Schiff base was described as shown in the Scheme 2. Also, the results from elemental analysis were in good agreement with the calculated values that confirmed this molecular formula of the ligand that formed in 1:1 molar ratio. The infrared spectrum of the ligand gave interesting peaks that predicting the successful preparation of the Schiff base ligand. The spectrum showed no strong absorption band at ~1760 cm^{-1} which indicated the absence of a ν(C=O) group of 2-acetylferrocene. Furthermore, a strong absorption band appeared at 1659 cm^{-1} that may be attributed to the ν(C=N) group. This was a good indication for the synthesis of novel organometallic Schiff base[21,22]. The band of N-pyridine appeared in the ligand[23] at 1108 cm^{-1}. Due to the preparation of Schiff base ligand was done in 1:1 molar ratio, so the spectrum showed a pair of intensity bands at 3389 and 3282 cm^{-1} which correspond to $\nu_{asy}(NH_2)$ and $\nu_{sym}(NH_2)$[24]. Also, it observed a band at 616 cm^{-1} which was corresponding to the $\nu(NH_2)_{bending}$[25]. The ^{1}H NMR spectrum of Schiff base ligand showed multiplet signals observed in the region of 4.23–4.77 ppm which attributed to the ferrocene protons. Also, a signal observed at 1.26 ppm was attributed to the methyl group[26]. The NH_2 proton signal appeared at 5.29 ppm in the ligand spectrum[27]. The aromatic protons (3H) of the ligand appeared as multiplet peaks at 6.56–7.69 ppm[28,29].

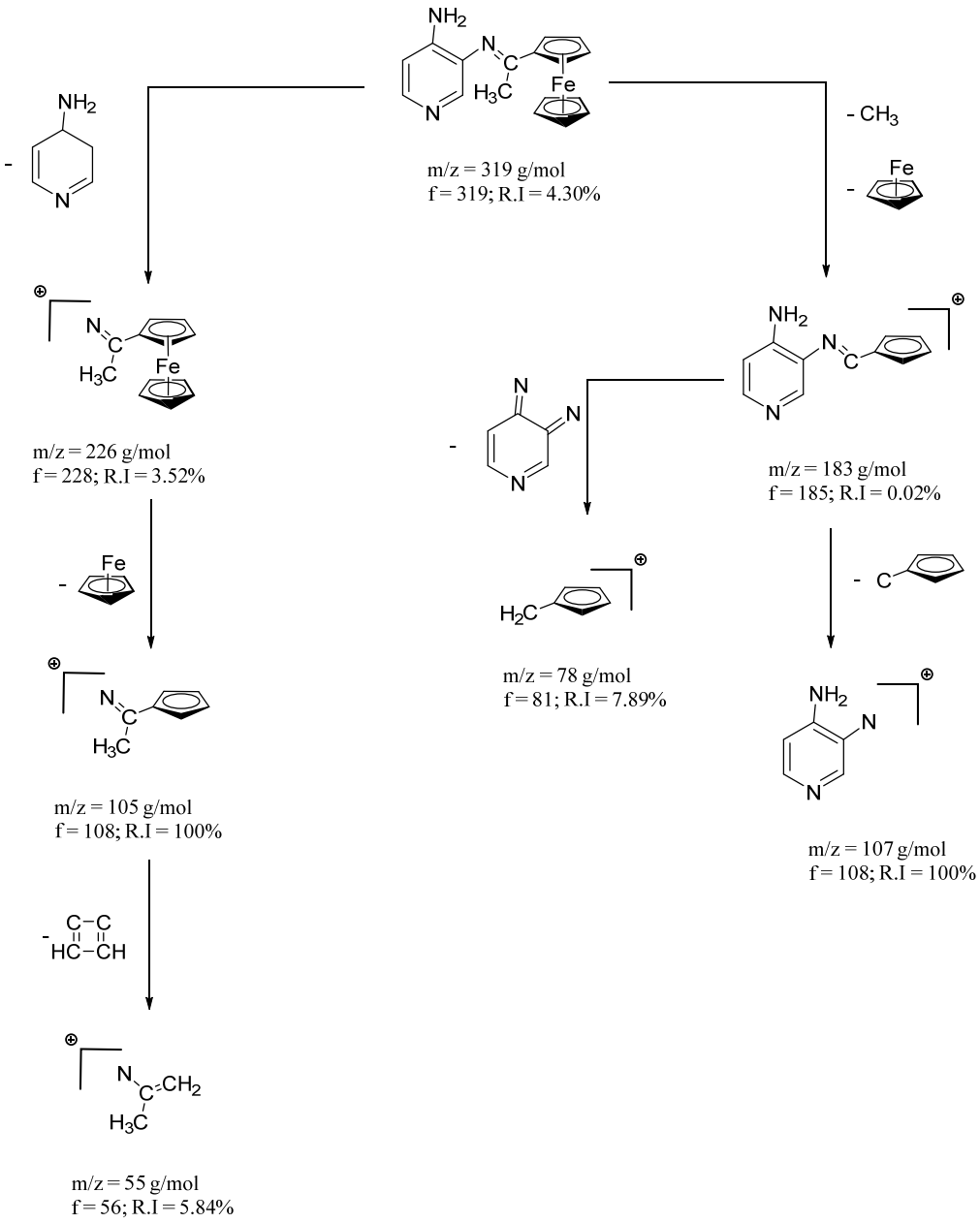

Proposed fragmentation pattern for prepared Schiff base ligand

Scheme 2

Geometrical optimization of the Schiff base ligand

The optimized structure of the synthesized organometallic Schiff base (L) as shown in Fig. 1. The bond angles and bond lengths were calculated and they were listed in Table 1[30]. The theoretical parameters such as dipole moment, total energy and energy of LUMO and HOMO orbitals were calculated. Additional parameters such as band gap energy, electrophilicity index (ω), chemical hardness (η), electronegativity (χ) and global softness (S)

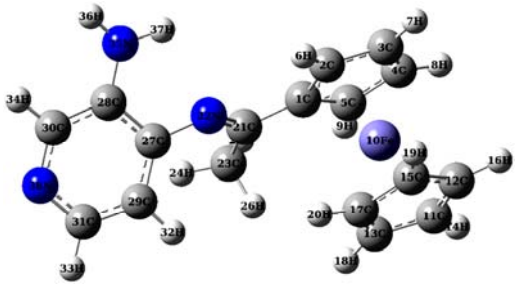

Fig. 1 — The optimized structure of organometallic Schiff base ligand (L).

Table 1 — The different optimized parameters (bond angles and bond lengths) of organometallic Schiff base ligand (L)

Bond angle (°)			
C(2)-C(1)-C(5)	107.3577	C(12)-Fe(10)-C(13)	66.6328
C(2)-C(1)-C(21)	125.3799	C(12)-Fe(10)-C(17)	66.7067
C(5)-C(1)-C(21)	127.2417	C(13)-Fe(10)-C(15)	66.6558
Fe(10)-C(1)-C(21)	124.4186	Fe(10)-C(11)-H(14)	125.2085
C(1)-C(2)-C(3)	108.2700	C(12)-C(11)-C(13)	107.9728
C(1)-C(2)-H(6)	124.4819	C(12)-C(11)-H(14)	125.9970
C(3)-C(2)-H(6)	127.2480	C(13)-C(11)-H(14)	126.0294
H(6)-C(2)-Fe(10)	124.7932	Fe(10)-C(12)-H(16)	124.9609
C(2)-C(3)-C(4)	108.1600	C(11)-C(12)-C(15)	107.9779
C(2)-C(3)-H(7)	125.9845	C(11)-C(12)-H(16)	126.0102
C(4)-C(3)-H(7)	125.8516	C(15)-C(12)-H(16)	126.0107
H(7)-C(3)-Fe(10)	125.1787	Fe(10)-C(13)-H(18)	125.5906
C(3)-C(4)-C(5)	108.0507	C(11)-C(13)-C(17)	108.0517
C(3)-C(4)-H(8)	126.0649	C(11)-C(13)-H(18)	125.9030
C(5)-C(4)-H(8)	125.8842	C(17)-C(13)-H(18)	126.0440
H(8)-C(4)-Fe(10)	125.4568	Fe(10)-C(15)-H(19)	124.5891
C(1)-C(5)-C(4)	108.1556	C(12)-C(15)-C(17)	108.0808
C(1)-C(5)-H(9)	126.3289	C(12)-C(15)-H(19)	126.0193
C(4)-C(5)-H(9)	125.5144	C(17)-C(15)-H(19)	125.8941
H(9)-C(5)-Fe(10)	125.1498	Fe(10)-C(17)-H(20)	124.2905
C(1)-Fe(10)-C(3)	66.6828	C(13)-C(17)-C(15)	107.9167
C(1)-Fe(10)-C(4)	66.8021	C(13)-C(17)-H(20)	126.1179
C(1)-Fe(10)-C(11)	141.3069	C(15)-C(17)-H(20)	125.9544
C(1)-Fe(10)-C(12)	178.9238	C(1)-C(21)-N(22)	117.3976
C(1)-Fe(10)-C(13)	113.8621	C(1)-C(21)-C(23)	117.1067
C(1)-Fe(10)-C(15)	139.3968	N(22)-C(21)-C(23)	125.4498
C(1)-Fe(10)-C(17)	112.9948	C(21)-N(22)-C(27)	126.4529
C(2)-Fe(10)-C(4)	66.6399	C(21)-C(23)-H(24)	111.6777
C(2)-Fe(10)-C(5)	66.9858	C(21)-C(23)-H(25)	109.7919
C(2)-Fe(10)-C(11)	178.6865	C(21)-C(23)-H(26)	110.9440
C(2)-Fe(10)-C(12)	139.0799	H(24)-C(23)-H(25)	108.5883
C(2)-Fe(10)-C(13)	140.5656	H(24)-C(23)-H(26)	108.5063
C(2)-Fe(10)-C(15)	112.1235	H(25)-C(23)-H(26)	107.1969
C(2)-Fe(10)-C(17)	112.7168	N(22)-C(27)-C(28)	116.4268
C(3)-Fe(10)-C(5)	66.6357	N(22)-C(27)-C(29)	125.5603
C(3)-Fe(10)-C(11)	140.240	C(28)-C(27)-C(29)	117.6620
C(3)-Fe(10)-C(12)	112.8117	C(27)-C(28)-C(30)	117.9341
C(3)-Fe(10)-C(13)	179.1987	C(27)-C(28)-H(35)	119.5194
C(3)-Fe(10)-C(15)	112.5438	C(30)-C(28)-H(35)	122.5430
C(3)-Fe(10)-C(17)	139.5826	C(27)-C(29)-H(31)	119.9577
C(4)-Fe(10)-C(11)	113.9462	C(27)-C(29)-H(32)	120.3358
C(4)-Fe(10)-C(12)	113.4822	H(31)-C(29)-H(32)	119.6704
C(4)-Fe(10)-C(13)	140.9860	C(28)-C(30)-H(34)	119.8373
C(4)-Fe(10)-C(15)	140.0021	C(28)-C(30)-H(38)	123.7812
C(4)-Fe(10)-C(17)	179.2522	H(34)-C(30)-H(38)	116.3786
C(5)-Fe(10)-C(11)	114.2478	C(29)-H(31)-N(33)	120.9632
C(5)-Fe(10)-C(12)	140.8086	C(29)-H(31)-H(38)	122.5866
C(5)-Fe(10)-C(13)	114.1642	N(33)-H(31)-H(38)	116.4499
C(5)-Fe(10)-C(15)	179.0755	C(28)-H(35)-N(36)	121.0840
C(5)-Fe(10)-C(17)	140.6784	C(28)-H(35)-C(37)	118.0521
C(11)-Fe(10)-C(15)	66.6408	N(36)-H(35)-C(37)	119.9089
C(11)-Fe(10)-C(17)	66.6885	C(30)-H(38)-H(31)	118.0533
Bond length (Å)			
C(1)-C(2)	1.4491	C(12)-H(16)	1.0810
C(1)-C(5)	1.4521	C(13)-C(17)	1.4440
C(1)-Fe(10)	2.1239	C(13)-H(18)	1.0812

Contd.

Table 1 — The different optimized parameters (bond angles and bond lengths) of organometallic Schiff base ligand (L) (*Contd.*)

Bond length (Å)			
C(1)-C(21)	1.4752	C(15)-C(17)	1.4415
C(2)-C(3)	1.4357	C(15)-H(19)	1.0810
C(2)-H(6)	1.0793	C(17)-H(20)	1.0810
C(2)-Fe(10)	2.1190	C(21)-N(22)	1.3067
C(3)-C(4)	1.4446	C(21)-C(23)	1.5235
C(3)-H(7)	1.0809	N(22)-C(27)	1.4108
C(3)-Fe(10)	2.1296	C(23)-H(24)	1.0924
C(4)-C(5)	1.4377	C(23)-H(25)	1.0963
C(4)-H(8)	1.0809	C(23)-H(26)	1.0984
C(4)-Fe(10)	2.1273	C(27)-C(28)	1.4314
C(5)-H(9)	1.0806	C(27)-C(29)	1.4122
C(5)-Fe(10)	2.1169	C(28)-C(30)	1.4174
Fe(10)-C(11)	2.1272	C(28)-H(35)	1.3846
Fe(10)-C(12)	2.1245	C(29)-H(31)	1.4062
Fe(10)-C(13)	2.1241	C(29)-H(32)	1.0862
Fe(10)-C(15)	2.1223	C(30)-H(34)	1.089
Fe(10)-C(17)	2.1224	C(30)-H(38)	1.3528
C(11)-C(12)	1.4426	H(31)-N(33)	1.0863
C(11)-C(13)	1.4424	H(35)-N(36)	1.0083
C(11)-H(14)	1.0811	H(35)-C(37)	1.0110
C(12)-C(15)	1.4433		

were also calculated for the ligand (L) according to the following equations and then represented in Table 2[31,32]:

$$\Delta E = E_{LUMO} - E_{HOMO} \quad \ldots(1)$$

$$\chi = \frac{-(E_{HOMO}+E_{LUMO})}{2} \quad \ldots(2)$$

$$\eta = \frac{E_{LUMO}-E_{HOMO}}{2} \quad \ldots(3)$$

$$\sigma = \frac{1}{\eta} \quad \ldots(4)$$

$$Pi = -\chi \quad \ldots(5)$$

$$S = \frac{1}{2\eta} \quad \ldots(6)$$

$$\omega = \frac{Pi^2}{2\eta} \quad \ldots(7)$$

$$\Delta N_{max} = -\frac{Pi}{\eta} \quad \ldots(8)$$

Chemical softness and hardness are significant parameters that measure the molecular stability and reactivity of the molecules. The small band gap energy indicated to highly reactive molecule while large band gap energy indicated to lower reactive molecule. The energy gap of the ligand was a very small value (3.82 eV) which indicated that the synthesized ligand is a very reactive molecule. The positive value of electrophilicity index (χ) and the negative value of chemical potential (Pi) indicated

that the ligand has a good tendency to form complexes with metal ions effectively.

Vibrational properties

In order to make a visual comparison between the calculated and observed vibrational frequencies, the theoretical FT-IR spectrum of the Schiff base ligand was calculated by B3LYP/ DFT method[33]. But the data of the vibrational frequencies that computed by quantum chemical methods such as DFT contain some systematic errors. So, using of scaling factor as 0.9648 for LanL2DZ to overcome these errors (which can be formed from harmonicity)[34] was carried out. Theoretical and experimental FT-IR spectroscopy for Schiff base was observed in Fig. 2. The experimental spectrum of the synthesized ligand showed characteristic bands at 3389, 3282, 1659, 1108 and 616 cm^{-1} which corresponding to $\nu_{asy}(NH_2)$, $\nu_{sym}(NH_2)$, azomethine group ν(C=N), N-pyridine ring and $\nu(NH_2)_{bending}$, respectively. The theoretical calculations also showed bands at 3617, 3283, 1662, 1123 and 618 cm^{-1}. These data gave good information about the successful condensation between 2-acetylferrocene and 3,4-diaminopyridine.

Table 2 — The different quantum chemical parameters of organometallic Schiff base ligand (L)

The calculated quantum chemical parameters	
E (a.u)	–945.58
Dipole moment (Debye)	5.07
E_{HOMO} (eV)	–5.58
E_{LUMO} (eV)	–1.76
ΔE (eV)	3.82
χ (eV)	3.67
η (eV)	1.91
σ $(eV)^{-1}$	0.52
Pi (eV)	–3.67
S $(eV)^{-1}$	0.26
ω (eV)	3.53
ΔN_{max}	1.92

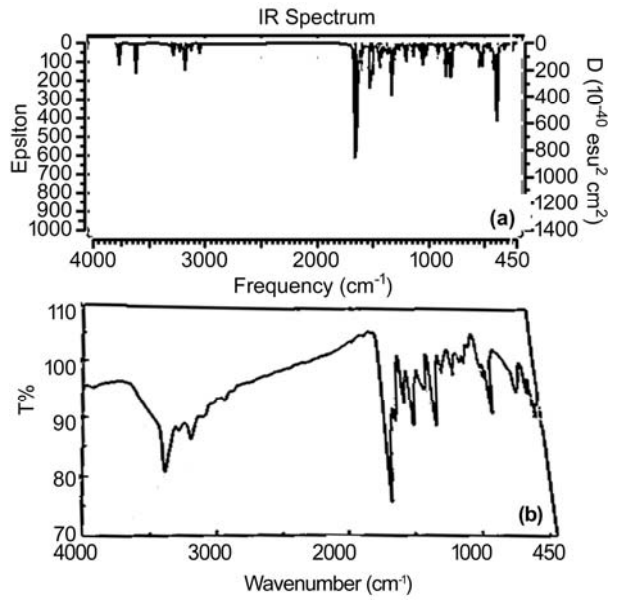

Fig. 2 — IR spectra of organometallic Schiff base ligand (L) (a) theoretical spectrum and (b) experimental spectrum.

UV-Visible analysis

From the data of DFT molecular orbital calculation for the synthesized Schiff base ligand, surface plots for the three lowest unoccupied molecular orbitals (LUMO, LUMO+2 and LUMO+4) and two highest occupied molecular orbital (HOMO and HOMO-3) were displayed to give visual evidence of the molecular orbitals that involved in the spectroscopic electronic energy transitions examined[35,36].

The electronic absorption spectral data of the organometallic Schiff base was recorded in 10^{-4} M DMF solution. This spectrum represented bands at 230 and 273 nm which related to the π–π* transitions of the ferrocene and benzene rings. The third absorption band appeared at λ_{max} = 306 nm that may correspond to the π–π* transition of the azomethine group[37,38].

The theoretical UV-Vis spectrum also showed three absorption bands: 238, 284 and 390 nm. The experimental and theoretical bands were shown in Fig. 3. The band appeared at 238 with oscillator strengths of f = 0.08 corresponded to the transition of HOMO to LUMO+4. The second peak computed at

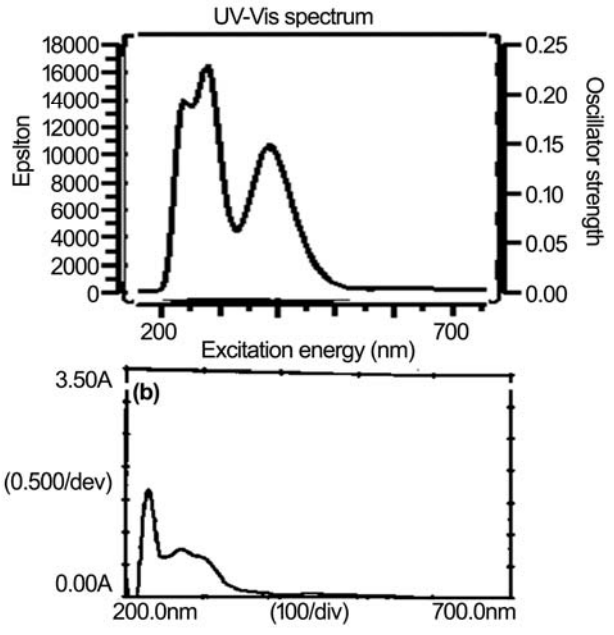

Fig. 3 — UV-Visible spectra of Schiff base ligand (L) (a) theoretical spectrum and (b) experimental spectrum.

284 nm with an oscillator strength of f = 0.20 was represented by the contribution of HOMO → LUMO+2. The Final peak appeared at 390 nm which corresponded to transition from HOMO-3 to LUMO with an oscillator strength of f = 0.02[33]. These data were listed in Table 3, and shown in Fig. 4.

Characterization of metal complexes

The condensation of 2-acetylferrocene with 3,4-diaminopyridine gave a new organometallic Schiff base (L). Then its Cr(III), Mn(II), Fe(III), Co(II), Ni(II), Cu(II), Zn(II) and Cd(II) complexes were prepared. These prepared compounds were also characterized by using different techniques such as elemental analysis (C, H, N and metal content), IR, ^{1}H NMR, molar conductance, UV-Vis, mass, SEM and thermal analyses (TG and DTG). The structure of Schiff base metal complexes was shown in Fig. 5.

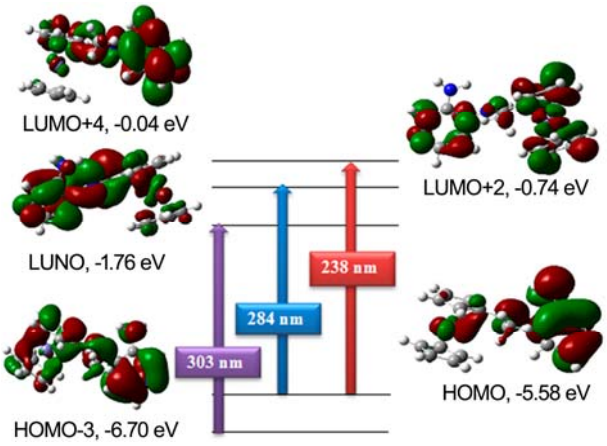

Fig. 4 — Theoretical electronic absorption transitions for Schiff base ligand (L) in methanol solvent.

Elemental analysis

The carbon, hydrogen, nitrogen and metal percentages with some physicochemical data were calculated. The colored solid complexes were then isolated. They were stable in air, having high melting points, insoluble in water and all complexes were soluble in DMF and DMSO but Mn(II), Co(II), Zn(II) and Cd(II) complexes were soluble also in ethanol and methanol. From these data, all compounds gave a good agreement with the calculated values and suggested that they were successfully prepared in a 1:1 metal-to-ligand stoichiometric ratio.

Molar conductivity measurements

Studying the conductivity of electrolytes in solutions is of great importance for gaining information about the intermolecular interactions existing in the solutions. So, the molar conductivity measurements of the Schiff base complexes were measured in 1×10^{-3} M solution. It was found that Fe(III), Cu(II), Zn(II) and Cd(II) complexes had non-electrolytic nature[39]. These results confirmed that all the chlorides are part of the coordination sphere.

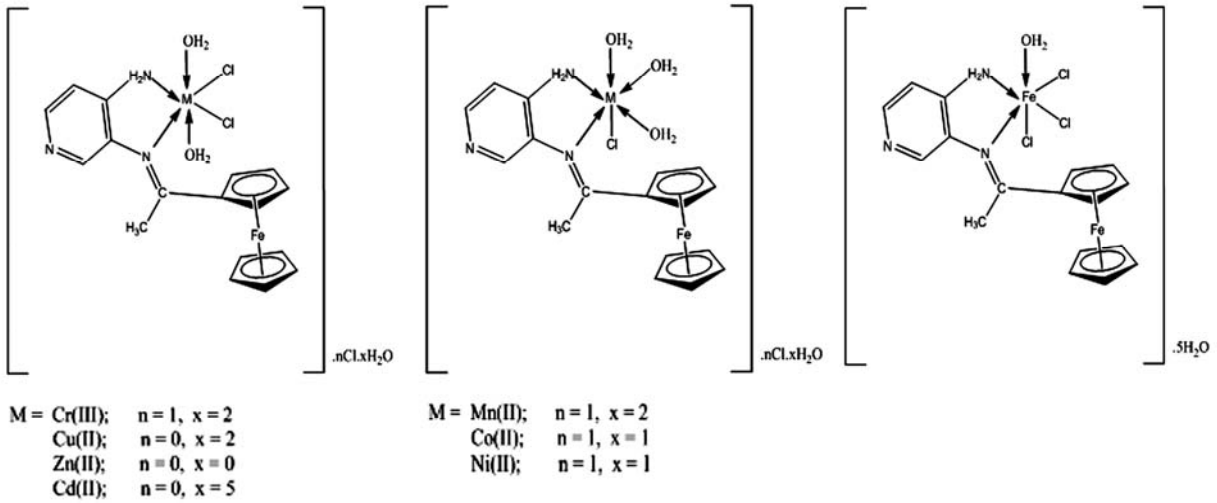

Fig. 5 — The proposed structure of organometallic Schiff base metal complexes.

Table 3 — Main calculated optical transitions with composite ion in terms of molecular orbitals

Compound	Transition	Excitation energy (eV)	λ_{max} calc. nm/(eV)	λ_{max} exp. nm/(eV)	Oscillator strength
Ligand (L)	HOMO ⟶ LUMO+4 (60%)	5.54	238 (5.22)	231 (5.36)	0.08
	HOMO ⟶ LUMO+2 (44%)	4.84	284 (4.36)	273 (4.53)	0.20
	HOMO-3 ⟶ LUMO (55%)	4.94	303 (4.09)	306 (4.04)	0.02

While, Cr(III), Mn(II), Co(II) and Ni(II) complexes have ionic nature and they were 1:1 electrolyte[40,41].

IR spectra

The FT-IR spectra of all metal complexes were compared with the spectrum of organometallic Schiff base in order to determine the involvement of the coordination positions in the chelation[42]. The spectrum of ligand showed some guide peaks which were beneficial in achieving this goal. The intensities and/or the positions of these peaks were expected to be changed upon chelation[43]. IR spectrum of the Schiff base ligand exhibited the most characteristic bands at 1659 cm^{-1} (ν(C=N), azomethine) and 616 cm^{-1} ($\nu(NH_2)_{bending}$). These data gave an important indication about the successful formation of the Schiff base ligand. The band at 1659 cm^{-1} due to the azomethine group of the Schiff base was shifted to lower frequencies (1638–1655 cm^{-1}) after complexation, indicated the bonding of nitrogen of the azomethine group to the metal ions[21]. Also, $\nu(NH_2)_{bending}$ band in the ligand was shifted to lower and higher frequencies (608–681 cm^{-1}) in all complexes. This indicated the bonding of nitrogen of amino group to metal ions[25]. The band of N-pyridine ring that appeared at 1108 cm^{-1} in the ligand spectrum was still in the complexes ~ at the same position (1106–1110 cm^{-1}). This indicated the non-participating of N-pyridine ring in the complexation[23]. The ligand spectrum showed a pair of intensity bands at 3389 and 3282 cm^{-1} which correspond to $\nu_{asy}(NH_2)$ and $\nu_{sym}(NH_2)$. Due to the presence of water molecules in the structure of all metal complexes, so these bands were included in a broad envelope band of OH group of these water molecules[35,44]. Also, two new bands at 878–980 and 800–877 cm^{-1} suggested the presence of coordinated water in all metal complexes. Furthermore, in lower frequency, new bands were found in the spectra of all complexes in the region 529–580 cm^{-1} which attributed to ν(M-O) stretching vibrations of coordinated water and in the region of 480–500 cm^{-1} which attributed to ν(M-N)[42,45–47]. Therefore, from the IR spectra of the Schiff base and its metal complexes, it was concluded that organometallic Schiff base behaved as neutral bidentate ligand and binds to the metal ions through azomethine-N and amino group-N.

^{1}H NMR spectra

The ^{1}H NMR spectra of organometallic Schiff base ligand and its Zn(II) complex were recorded to confirm their structural. These spectra of the prepared compounds were recorded in DMSO-d_6 solution, using tetramethylsilane (TMS) as internal standard[48,49]. The ^{1}H NMR spectrum of Schiff base showed multiplet signals observed in the region of 4.23–4.77 ppm which attributed to the ferrocene protons. These signals appeared in Zn(II) complex at the region of 4.20–4.75 ppm. Also, a signal observed at 1.26 and 1.20 ppm can attribute to methyl group in ligand and Zn(II) complex, respectively[26]. The aromatic protons (3H) of the ligand was shown as multiplet peaks at 6.56–7.69 ppm. These peaks still appeared in the Zn(II) complex at 6.26–7.58 ppm[28,29]. The NH_2 proton signal appeared in the ligand at 5.29 ppm. This band shifted to a lower value at 4.96 ppm in the Zn(II) complex, indicating the involvement of the NH_2 group in coordination[27].

Scanning electron microscope (SEM)

The scanning electron microscopy (SEM) is a simple method that can be used to check the deposited samples which successfully indicated that the nanoparticles have been formed. So, the prepared Schiff base ligand and its Cd(II) complex were checked by SEM analysis[40,50]. According to the images of SEM for the ligand and its complex that was shown in Fig. 6, the diameter and the shape of these compounds were reported. From these data, it was clear that the scanning electron microscopy picture of the ligand was like mushroom structure with average particle size 53 nm. While the Cd(II) complex appeared as plates with an average particle size 28 nm. It was obvious that the particle size of the complex was smaller than the Schiff base ligand, which can be used as good precursors in the formation of metal complex nanoparticles. The difference in the shape and the size of the Schiff base than its metal complex was mainly dependent on the presence of metal ion[51,52].

UV-Visible spectra of the Schiff base ligand and its metal complexes

The electronic absorption spectra (UV–Vis) of the synthesized Schiff base and its metal complexes were measured at room temperature at 1×10^{-4} M, in the range of 200–700 nm. There are three bands appeared in the absorption spectrum of the ligand at 230, 273 and 306 nm. The first and second bands related to the π-π* transitions of the ferrocene and benzene rings. While the third band appeared at λ_{max} = 306 nm that may correspond to the π–π* transition of the azomethine group[37]. In metal complexes, the UV-spectral bands were listed in Table 4 which showed

shifting to lower or higher value than the free ligand. The first band which corresponded to π-π* transitions of the ferrocene and benzene rings was shifted to 231–297 nm. While the other band that related to π–π* transition of the azomethine group was shifted to 300–302 nm, confirmed the coordination of the azomethine nitrogen to the metal ions[53,54].

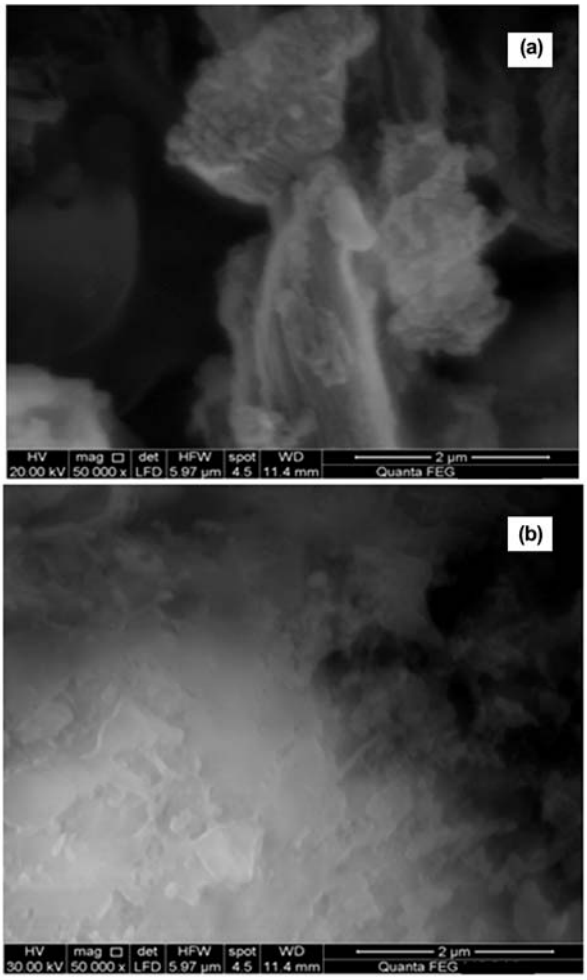

Fig. 6 — The SEM images of the nanoparticles produced a) organometallic Schiff base ligand (L) and b) $[Cd(L)(H_2O)_2Cl_2]5H_2O$ complex.

Table 4 — The UV-spectral bands and transitions of Schiff base ligand and its metal complexes

Compound	π–π* (ferrocene and benzene rings)	π–π* (azomethine group)
Schiff base ligand (L)	230, 273	306
$[Cr(L)(H_2O)_2Cl_2]Cl.2H_2O$	265	…….
$[Mn(L)(H_2O)_3Cl]Cl.2H_2O$	231	301
$[Fe(L)(H_2O)Cl_3]5H_2O$	263	…….
$[Co(L)(H_2O)_3Cl]Cl.H_2O$	231	302
$[Ni(L)(H_2O)_3Cl]Cl.H_2O$	231, 297	…….
$[Cu(L)(H_2O)_2Cl_2]2H_2O$	265	…….
$[Zn(L)(H_2O)_2Cl_2]$	231, 275	300
$[Cd(L)(H_2O)_2Cl_2]5H_2O$	231, 276	…….

Thermal analysis of Schiff base ligand and its metal complexes

Thermal analysis is a very important and useful technique that used to assess the thermal stability of materials, identify the different types of the solvent of crystallization and confirm molecular structures. The thermal analysis was investigated at a heating rate of 10 °C/min in a nitrogen atmosphere over the range from ambient temperature to 1000 °C. The observed and the calculated data of DTG/TG peaks are summarized in Table 5.

The Schiff base ligand with the molecular formula ($C_{17}H_{17}N_3Fe$) was thermally decomposed in one decomposition step. This step with estimated mass loss of 82.09% (calculated mass loss = 82.45%) within the temperature range 105–850 °C may correspond to the loss of $C_{17}H_{17}N_3$ molecule. The DTG curve gave the maximum peak temperature at 202 °C. At the end of decomposition Fe remain as residue. The overall weight loss amounted to 82.09% (calculated mass loss = 82.45%).

The $[Cr(L)(H_2O)_2Cl_2]Cl.2H_2O$ complex was thermally decomposed in four steps. The first and second steps with estimated mass loss of 21.04% (calculated mass loss = 21.29%) within the temperature range 40-370 °C correspond to a loss of Cl_2 gas, one molecule of water of hydration and C_2H_4 molecule. The DTG curve gave exothermic peaks at 90 and 241 °C (the maximum peak temperature). The third and fourth steps correspond to an estimated mass loss of 36.59% (calculated mass loss = 36.49%) within the temperature range 370–1000 °C and represented the loss of HCl and $C_8H_{18}N_3O_{0.5}$ molecules, leaving FeO and ½ Cr_2O_3 contaminated with carbon as residues. The DTG curve of the third and fourth steps gave peaks at 418 and 914 °C. The overall weight loss amounted to 57.63% (calculated mass loss = 57.78%).

In the thermograph of $[Mn(L)(H_2O)_3Cl]Cl.2H_2O$ complex, the first step displayed a gradual mass loss of 6.62% (calculated mass loss = 6.73%) within the temperature range of 40–140 °C which may correspond to the loss of two molecules of water of hydration. The DTG curve gave a peak at 70 °C (the maximum peak temperature). The second step indicated a mass loss of 32.11% (calculated mass loss = 32.15%) which corresponded to a loss of H_2O, Cl_2 and C_5H_9N molecule within temperature range 140–195 °C. The maximum peak temperature was at

Table 5 — Thermoanalytical results (TG and DTG) of organometallic Schiff base (L) and its metal complexes

Complex	TG range (°C)	DTG_{max} (°C)	n*	Mass loss Estim (Calc.) %	Total mass loss	Assignment	Residues
Schiff base ligand (L)	105–850	202	1	82.09 (82.45) (82.45)	82.09	-Loss of $C_{17}H_{17}N_3$.	Fe
$[Cr(L)(H_2O)_2Cl_2]Cl.2H_2O$	40–370	90, 241	2	21.04 (21.29)		-Loss of Cl_2, H_2O and C_2H_4.	$FeO + {}^1/_2Cr_2O_3$
	370–1000	418, 914	2	36.59 (36.49) (57.78)	57.63	-Loss of HCl and $C_8H_{18}N_3O_{0.5}$.	7C
$[Mn(L)(H_2O)_3Cl]Cl.2H_2O$	40–140	70	1	6.62 (6.73)		-Loss of $2H_2O$.	
	140–195	179	1	32.11 (32.15)		-Loss of H_2O, Cl_2 and C_5H_9N.	
	195–535	523	1	10.27 (10.28)		-Loss of C_4H_7.	
	535–1000	823	1	24.60 (24.11) (73.27)	73.60	-Loss of $C_8H_5N_2$.	FeO+MnO
$[Fe(L)(H_2O)Cl_3]5H_2O$	35–155	87	1	8.88 (9.16)		.-Loss of $3H_2O$.	
	155–535	180, 376	2	20.83 (20.61)		-Loss of $C_5H_{12}NCl$.	$FeO+{}^1/_2Fe_2O_3$
	535–1000	638, 793	2	25.86 (26.12) (55.89)	55.57	-Loss of 2HCl, $C_3H_9N_2O_{0.5}$.	+9C
$[Co(L)(H_2O)_3Cl]Cl.H_2O$	30–95	78	1	3.62 (3.45)		-Loss of H_2O.	
	95–180	171	1	17.48 (17.08)		-Loss of H_2O and Cl_2.	
	180–520	385	1	29.93 (30.13)		-Loss of $C_{10}H_9N_2$.	
	520–1000	646	1	18.34 (18.81) (69.47)	69.34	-Loss of $C_6H_{12}N$.	FeO+CoO+C
$[Ni(L)(H_2O)_3Cl]Cl.H_2O$	30–160	81	1	9.91 (10.27)		-Loss of H_2O and ½ Cl_2.	
	160–670	250, 455	2	20.75 (20.63)		-Loss of H_2O and C_4H_6Cl.	
	670–1000	827, 890	2	31.47 (31.67) (62.57)	62.13	-Loss of $C_9H_{15}N_3$.	FeO+NiO+4C
$[Cu(L)(H_2O)_2Cl_2]2H_2O$	30–150	78	1	15.48 (15.22)		-Loss of $2H_2O$ and C_2H_6N.	
	150–570	152	1	24.36 (24.17)		-Loss of C_3H_6N and Cl_2.	
	570–1000	577, 750	2	22.54 (22.65) (62.04)	62.38	-Loss of C_8H_9N.	FeO+CuO+4C
$[Zn(L)(H_2O)_2Cl_2]$	90–265	197	1	36.12 (36.05)		-Loss of Cl_2 and C_7H_8N.	
	265–500	410	1	10.81 (11.00)		-Loss of C_3H_4N.	
	500–1000	578, 707	2	21.46 (21.79) (68.84)	68.39	-Loss of C_7H_9N.	FeO+ZnO
$[Cd(L)(H_2O)_2Cl_2]5H_2O$	30–240	83, 188	2	43.68 (44.03)		-Loss of $5H_2O$ and $C_{11}H_5NCl$.	
	240–410	329	1	17.05 (17.12)		-Loss of HCl and $C_3H_7N_2$.	
	410–1000	601, 861	2	7.31 (7.01) (68.16)	68.04	-Loss of C_3H_8.	CdO+FeO

n* = number of decomposition steps

179 °C. The third step showed a mass loss of 10.27% (calculated mass loss = 10.28%) which corresponded to a loss of C_4H_7 molecule within temperature range 195–535 °C. The maximum peak temperature was at 523 °C. The final step corresponded to a loss of $C_8H_5N_2$ with estimated mass loss = 24.60% (calculated mass loss = 24.11%) within a temperature range from 535 °C to 1000 °C. The maximum peak temperature was found at 823 °C. Finally, FeO + MnO remained as residues. The overall weight loss amounted to 73.60% (calculated mass loss = 73.27%).

The $[Fe(L)(H_2O)Cl_3]5H_2O$ complex showed five decomposition steps within the range 35–1000 °C. The first decomposition step was accompanied by loss of $3H_2O$ molecules in the range 35–155 °C with an estimated mass loss of 8.88% (calculated mass loss = 9.16%). The DTG curve gave a peak at 87 °C (the maximum peak temperature). The second and third steps of decomposition corresponded to a loss of $C_5H_{12}NCl$ molecule at 155–535 °C with an estimated mass loss of 20.83% (calculated mass loss = 20.61%) with maximum peaks temperature at 180 and 376 °C. The final two decomposition steps within the range 535–1000 °C were assigned to loss of 2HCl and $C_3H_9N_2O_{0.5}$ molecules with a mass loss of 25.86% (calculated mass loss = 26.12%). Ferric and ferrous oxides contaminated with carbon remained as residues. The overall weight loss amounted to 55.57% (calculated mass loss = 55.89%).

In the thermograph of $[Co(L)(H_2O)_3Cl]Cl.H_2O$ complex, the first step of decomposition displayed a gradual mass loss of 3.62% (calculated mass loss =

3.45%) within the temperature range of 30–95 °C which may be correspond to the loss of one molecule of water of hydration. The DTG curve gave a peak at 78 °C (the maximum peak temperature). The second step showed a mass loss of 17.48% (calculated mass loss = 17.08%) which corresponded to a loss of H_2O and Cl_2 gas within temperature range 95–180 °C. The maximum peak temperature was at 171 °C. The third step showed a mass loss of 29.93% (calculated mass loss = 30.13%) which corresponded to a loss of $C_{10}H_9N_2$ molecule within temperature range 180–520 °C. The maximum peak temperature was at 385 °C. The final step corresponds to a loss of $C_6H_{12}N$ with estimated mass loss = 18.34% (calculated mass loss = 18.81%) within temperature range 520–1000 °C. The maximum peak temperature was found at 646 °C. Finally FeO and CoO contaminated with carbon remained as residues. The overall weight loss amounted to 69.34% (calculated mass loss = 69.47%).

The $[Ni(L)(H_2O)_3Cl]Cl.H_2O$ complex lost upon heating H_2O and $½Cl_2$ molecules in the first step of decomposition within the temperature range of 30-160 °C, at maximum peak temperature at 81 °C with estimated mass loss of 9.91% (calculated mass loss = 10.27%). The second and third steps accounted for the loss of H_2O and C_4H_6Cl molecules within the temperature range of 160–670 °C, at maximum peaks temperature at 250 and 455 °C, with estimated mass loss of 20.75% (calculated mass loss = 20.63%). The final two steps corresponded to a loss of $C_9H_{15}N_3$ molecule within temperature range 670–1000 °C at maximum peaks temperature at 827 and 890 °C, with estimated mass loss of 31.47% (calculated mass loss = 31.67%), leaving FeO and NiO contaminated with carbon as residues of decomposition. The overall weight loss amounted to 62.13% (calculated mass loss = 62.57%).

The $[Cu(L)(H_2O)_2Cl_2]2H_2O$ complex gave decomposition pattern started at 30 °C and finished at 1000 °C with three stages. The first stage was one step within the temperature range of 30–150 °C with maximum temperature at 78 °C which represented the loss of $2H_2O$ (hydrated) and C_2H_6N molecule with a found mass loss of 15.48% (calculated mass loss = 15.22%). The second stage was one step which represented the loss of Cl_2 gas and C_3H_6N molecule with a mass loss of 24.36% (calculated mass loss = 24.17%) within the temperature range 150–570 °C and maximum peak temperature at 152 °C. The final stage was two steps which represented the loss of C_8H_9N molecule with a mass loss of 22.54% (calculated mass loss = 22.65%) within the temperature range 570–1000 °C and maximum peaks temperature at 577 and 750 °C. At the end of the thermogram, the metal oxide CuO and FeO contaminated with carbon remained as residues. The overall weight loss amounted to 62.38% (calculated mass loss = 62.04%).

In the thermograph of $[Zn(L)(H_2O)_2Cl_2]$ complex, the first step of decomposition corresponds to mass loss of 36.12% (calculated mass loss = 36.05%) within the temperature range 90–265 °C with a maximum peak temperature at 197 °C, represented the loss of Cl_2 gas and C_7H_8N molecule. The second step occurred within the temperature range 265-500 °C with a maximum peak temperature at 410 °C may be attributed to the decomposition of C_3H_4N molecule with found mass loss of 10.81% (calculated mass loss = 11.00%). The third and fourth steps started at 500 °C and ended at 1000 °C with maximum peaks temperature at 578 and 707 °C and may be accounted to the loss of C_7H_9N molecule with mass loss of 21.46% (calculated mass loss = 21.79%), leaving behind ZnO and FeO oxides as residues of decomposition. The overall weight loss amounted to 68.39% (calculated mass loss = 68.84%).

The $[Cd(L)(H_2O)_2Cl_2]5H_2O$ complex upon heating lost $5H_2O$ and $C_{11}H_5NCl$ molecules in the first and second steps of decomposition within the temperature range 30–240 °C at maximum peaks temperature 83 and 188 °C, with a mass loss = 43.68% (calculated mass loss = 44.03%). The third step of decomposition occurred at maximum peak temperature at 329 °C, corresponding to a loss of $C_3H_7N_2$ and HCl molecules with a mass loss = 17.05% (calculated mass loss = 17.12%), in the temperature range of 240–410 °C. The final two steps started decomposition at 410 °C and ended at 1000 °C with maximum peaks temperature at 601 and 861 °C and may be correspond to the loss of C_3H_8 molecule with mass loss of 7.31% (calculated mass loss = 7.01%), leaving CdO and FeO oxides as residues of decomposition. The overall weight loss amounted to 68.04% (calculated mass loss = 68.16%).

Structural interpretation

The structure of the prepared Cr(III), Mn(II), Fe(III), Co(II), Ni(II), Cu(II), Zn(II) and Cd(II) complexes were characterized by different techniques such as elemental analysis (C, H, N, M), molar conductivity, FT-IR, UV-Vis, ^{1}H NMR, SEM, mass spectral and thermal analyses. Accordingly, the

structure of all complexes could be proposed as shown in Fig. 5.

Antimicrobial activities

The organometallic Schiff base (L) and its metal complexes were evaluated for antibacterial and antifungal activities against two strain of Gram-positive bacteria (*Bacillus subtilis* and *Staphylococcus aureus*), two strain of Gram-negative bacteria (*Escherichia coli* and *Salmonella typhimurium*) and two pathogenic fungi (*Aspergillus fumigatus* and *Candida albicans*). The efficiencies of antibacterial and antifungal activities were compared with standard antibiotics Gentamycin and Ketokonazole, respectively, and then shown in Fig. 7[55].

Also, the activities of these compounds against Gram-positive and Gram-negative bacteria were confirmed by calculating the activity index according to the following relation[56,57].

Activity index (A) = [Inhibition Zone of compound (mm) / Inhibition Zone of standard drug (mm)]×100 …(9)

From the results, it was concluded that ligand, Mn(II) and Ni(II) complexes had no activity index against all species, while Co(II), Cu(II), Zn(II) and Cd(II) complexes had very high activity index[58] (Fig. 8).

By comparing the results of biological activities of the Schiff base ligand and its metal complexes, it was indicated that the ligand, Mn(II) and Ni(II) complexes were biologically inactive against all four different bacteria species. Also, Cr(III) and Fe(III) complexes were biologically inactive except against *E.coli* species with inhibition zone diameter values 12 and 10 mm/mg, respectively. While Co(II), Cu(II), Zn(II) and Cd(II) complexes showed very high bacterial activities against four species of bacteria. Furthermore, the antifungal activities of the ligand indicated its biological inactive against *Aspergillus fumigatus* species and biologically active against *Candida albicans* species with inhibition zone diameter value 15 mm/mg. Almost of metal complexes were inactive against two fungal species except for Cd(II) complex which had fungicidal activity against two fungal species. Also, Cr(III) and Cu(II) complexes were active against only *Candida albicans.* Co(II) complex had fungicidal activity against *Aspergillus fumigatus species* only.

According to Tweedy's theory[59], the polarity of the metal atom was reduced by chelation. The reason for this reduction is due to partial sharing of metal atom's positive charge with a donor group and the delocalization of π-electron over the whole chelate ring. By this chelation, the lipophilic character of the central metal atom would be enhanced which subsequently prefers its permeation through the lipid layers of the cell membrane and then the metal binding sites would be blocked on enzymes of microorganism[60,61].

Anticancer activities

In recent research, the discovery of metal-based anticancer drug is considered as one of the most advanced areas in life[62,63]. So, the breast cancer cell line (MCF-7) was used to determine the antiproliferative effect of the prepared organometallic Schiff base ligand and its metal complexes. In addition, melanocyte cell line (HFB-4) was also used as a model

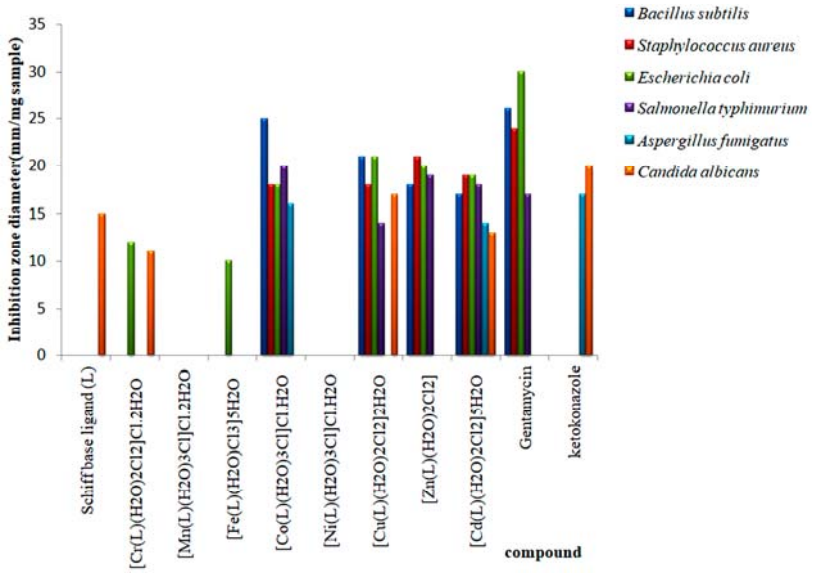

Fig. 7 — Biological activity of organometallic Schiff base ligand (L) and its metal complexes.

for normal cells[64]. Firstly all the prepared compounds were screened against single dose experiment with concentration 100 µg/mL on MCF-7 cell line. The results indicated that the ligand had inhibition ratio value of 67%, while its metal complexes values were between 61–78%. Furthermore, the four concentrations (5, 12.5, 25 and 50 µg/mL) and the median inhibitory concentration (IC_{50}) values of the compounds with the inhibition ratio value >70% were detected. These compounds were showed in Fig. 9. From these data, it showed that the Cd(II) complex had the lowest IC_{50} value = 22.2 µg/mL. It considered as the most active compound against MCF-7 cell line. This conclusion was confirmed by screening these active compounds against normal HFB-4 cell line at concentration

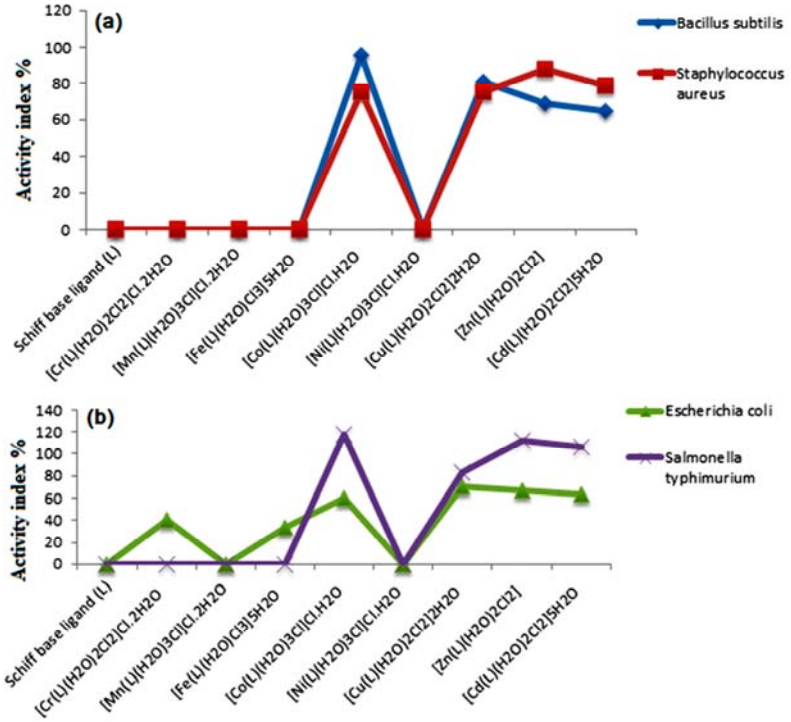

Fig. 8 — Activity index of organometallic Schiff base ligand (L) and its metal complexes against (a) different Gram positive bacteria species and (b) different Gram negative bacteria species.

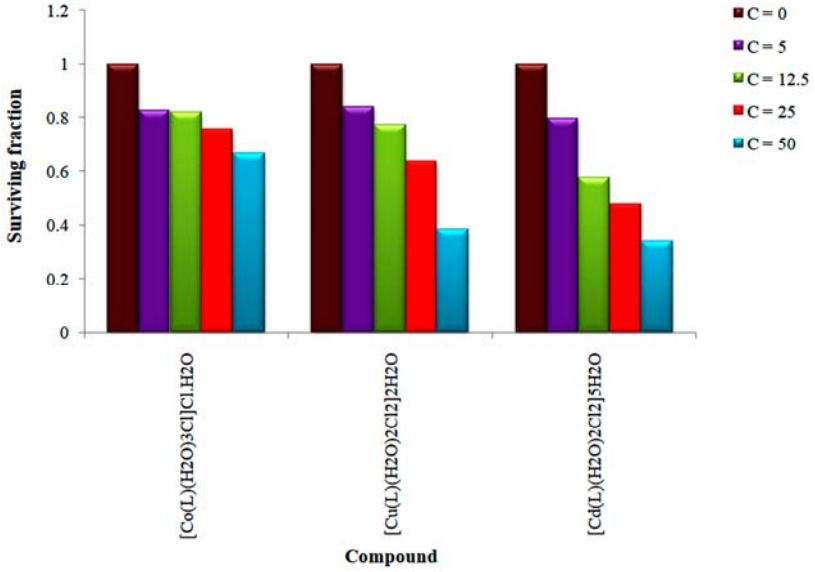

Fig. 9 — Anticancer activity against breast cancer of the ligand (L) and its metal complexes.

100 μg/mL. It showed that Cd(II) complex had the highest surviving ratio value = 67%. So, Cd(II) complex can be considered as a promising drug for breast cancer with low cytotoxic effect.

Molecular modeling of organometallic Schiff base ligand (L) and its Cd(II) complex: Docking study

The technique of molecular docking has played a vital role in understanding the interactions between drugs and DNA for drug design and discovery. Also, it can be used in the mechanistic study by replacing a new small molecule in the binding site of the target-specific region that presents in DNA[65–67]. The optimized structure of the Schiff base ligand and its Cd(II) complex were docked with three possible biological targets: the receptors of breast cancer mutant oxidoreductase (PDB ID: 3HB5), Colon Cancer Antigen 10 from *Homo sapiens* (PDB ID: 2HQ6) and a mutant human androgen receptor (ARccr) derived from an androgen-independent prostate cancer (PDB ID: 1GS4). Three-dimensional structures of docking were shown in Fig. 10. Also, the binding energies of the organometallic Schiff base ligand and its Cd(II) complex with the three receptors were calculated using computational docking studies and then were listed in Table 6[68,69]. From the results of docking studies, It is shown that there are possible

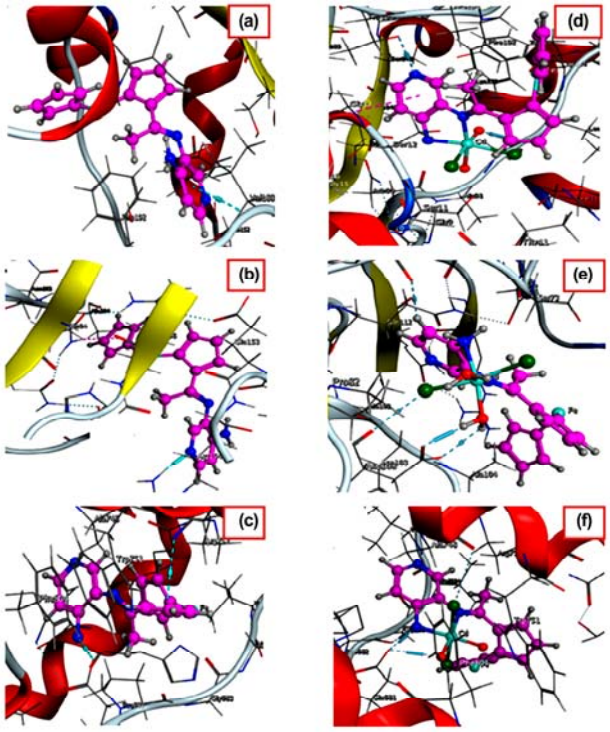

Fig. 10 — 3D structure of the interaction between Schiff base ligand (L) with receptors of (a) 3HB5, (b) 2HQ6, and, (c) 1GS4 and 3D plot of the interaction between $[Cd(L)(H_2O)_2Cl_2]5H_2O$ complex with receptors of (d) 3HB5, (e) 2HQ6, and, (f) 1GS4.

Table 6 — Energy values obtained in docking calculations of Schiff base ligand (L) and its Cd(II) complex with receptors of breast cancer mutant oxidoreductase (PDB ID: 3HB5), Colon Cancer Antigen 10 from Homo Sapiens (PDB ID: 2HQ6) and a mutant human androgen receptor (ARccr) derived from an androgen-independent prostate cancer (PDB ID: 1GS4)

Compound	Receptor	Ligand moiety	Receptor site	Interaction	Distance (A°)	E (kcal mol^{-1})
Ligand (L)	3HB5	C4	NZ LYS 159 N	ionic	3.15	–3.60
		6-ring	VAL 188	π-H	4.38	–0.70
	2HQ6	N33	NH1 ARG 154	H-acceptor	3.14	–4.90
		5-ring	NE2 GLN 64	π-H	4.35	–0.70
	1GS4	N30	OE2 GLU 681	H-donor	3.28	–1.10
		C16	NH2 ARG 752	ionic	3.63	–1.40
		C34	6-ring TRP 718	H-π	4.11	–1.00
		5-ring	NH2 ARG 752	π-cation	3.85	–0.70
Cd (II) complex	3HB5	O37	O GLY 92	H-donor	2.64	–13.90
		N43	OG1 THR 190	H-acceptor	2.94	–0.90
		C4	NH2 ARG 37	ionic	3.47	–2.00
	2HQ6	C28	O GLY 75	H-donor	3.28	–0.80
		CL35	O ASP 108	H-donor	3.26	–1.00
		O40	OD1 ASP 108	H-donor	2.88	–21.10
		O40	OD2 ASP 108	H-donor	2.92	–1.40
		O37	OD1 ASP 108	Ionic	3.89	–0.70
		O40	OD1 ASP 108	ionic	2.88	–5.30
		O40	OD2 ASP 108	ionic	2.92	–5.00
	1GS4	N31	OE2 GLU 681	H-donor	2.91	–11.10
		N31	O PRO 682	H-donor	2.90	–11.50
		CL36	O ALA 748	H-donor	3.83	–0.50
		O37	OE2 GLU 681	H-donor	2.77	–19.30
		N31	OE2 GLU 681	Ionic	2.91	–5.10
		O37	OE2 GLU 681	Ionic	2.77	–6.20

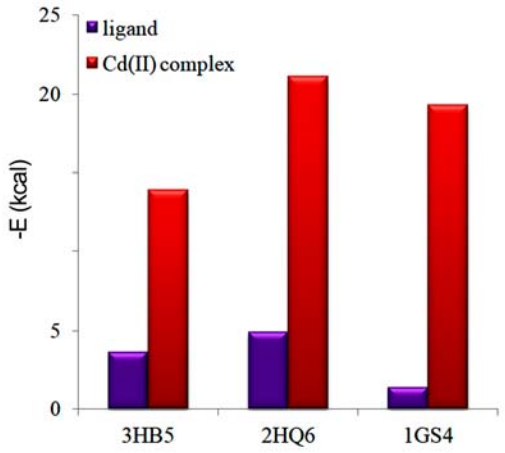

Fig. 11— The relation between The lowest binding energy of the ligand and its Cd(II) complex with 3HB5, 2HQ6 and 1GS4 receptors.

interactions between Schiff base ligand (L) and its Cd(II) complex with the three receptors. The data detected that the main interaction forces of the Schiff base ligand with the active sites were H-acceptor, H-donor, ionic, H-π and π-cation. Furthermore, the lowest binding energies of the Schiff base ligand and its Cd(II) complex with three receptors were calculated and then showed in Fig. 11. The minimum binding energies for ligand were found to be −3.6, –4.9 and −1.4 kcal mol^{-1} and to be –13.9, –21.1 and –19.3 kcal mol^{-1} for $[Cd(L)(H_2O)_2Cl_2]5H_2O$ complex with 3HB5, 2HQ6 and 1GS4, respectively. The complexation caused the decreasing in binding energy. As a result, it was shown that the binding energies of Cd(II) complex were lower than the parent ligand. The strongest binding of the complex was with the 2HQ6 receptor, it had the lowest binding energy value (–21.1 kcal mol^{-1}) than the other receptors.

Conclusions

The present study describes in the synthesis of a novel organometallic Schiff base ligand (L) and its Cr(III), Mn(II), Fe(III), Co(II), Ni(II), Cu(II), Zn(II) and Cd(II) complexes. The ligand has been prepared by condensation of 2-acetylferrocene with 3,4-diaminopyridine. These compounds were characterized by different spectroscopic methods. The results obtained can be summarized as follows:

(1) From infrared spectra, the successful synthesis of the ligand could be detected and it has behaved as a neutral bidentate ligand in all metal complexes. The coordination bonds occurred with metal ions through azomethine nitrogen and NH_2 group.

(2) Elemental analysis indicated that reaction between ligand and metal ions occurred at 1:1 molar ratio. Also, all complexes had octahedral structures.

(3) From conductivity results, it was observed that Cr(III), Mn(II), Co(II) and Ni(II) complexes were electrolytes while other complexes were non-electrolytes.

(4) The prepared compounds were screened against breast cancer (MCF-7) and human normal melanocytes (HFB-4) cell lines. From the results, it showed that Cd(II) complex had the lowest IC_{50} value = 22.2 µg/mL against MCF-7 cell line. So, it was considered as the most active compound that can be used as a very active drug with low cytotoxic effect.

(5) The biological activity of the synthesized ligand and its metal complexes against four different bacterial species showed that most prepared compounds were biologically inactive except Co(II), Cu(II), Zn(II) and Cd(II) complexes.

(6) Quantum chemical parameters using the DFT method for bond lengths, bond angles, dipole moment, total energy and energy of HOMO and LUMO orbitals were calculated.

(7) Molecular docking studies were also carried out for the parent Schiff base ligand (L) and its Cd(II) complex with different receptors. The data showed that the binding energies of Cd(II) complex were lower than the parent ligand. The strongest binding of the complex was with the 2HQ6 receptor as it had the lowest binding energy value (-21.1 kcal mol^{-1}) compared to the other receptors.

References

1 Shahzadi R S, Ali S, Parvez M, Badshah A, Ahmed E & Malik A, *Russian J Inorg Chem*, 52 (2007) 386.
2 Bhardwaj C N & Singh V R, *Indian J Chem*, 33A (1994) 423.
3 Ekennia A C, Osowole A A, Olasunkanmi L O, Onwudiwe D C, Olubiyi O O & Ebenso E E, *J Mol Str*, 1150 (2017) 279.
4 Ceyhan G, Celik C, Urus S, Demirtas I, Elmastas M & Tumer M, *Spectrochim Acta A,* 81 (2011) 184.
5 Vassylyev O, *Molecules*, 10 (2005) 585.
6 Wilkinson G, *J Organomet Chem*, 100 (1975) 273.
7 Najafabadi B K, Hesari M, Workentin M S & Corrigan J F, *J Organomet Chem,* 703 (2012) 16.
8 Li Y F & Liu Z Q, *Eur J Pharma Sci,* 44 (2011) 158.
9 Tirkey V, Mishra S, Dash H R, Das S, Nayak B P, Mobin S M & Chatterjee S, *J Organomet Chem,* 732 (2013) 122.
10 Raman O N, Sakthivel A, Raja J D & Rajasekaran K, *Russian J Inorg Chem,* 53 (2008) 213.

11 Deveci P & Arslan U, *J Organomet Chem,* 696 (2011**)** 3756.
12 Aly M R E, El Azab I H & Gobouri A A, *Monatsh Chem*, 149 (2018**)** 505.
13 Bauer A W, Kirbay W A W, Sherris J S, Turk M, *Am J Clin Pathol*, 45 (1966) 493.
14 Chandra S, Jain D, Sharma A K & Sharma P, *Molecules,* 14 (2009) 174.
15 Skehan P, Storeng R, Scudiero D, Monks A, McMahon J, Vistica D, Warren J T, Bokesch H, Kenney S & Boyd M R, *J Nat Cancer Instit,* 82 (1990) 1107.
16 Becke A D, *J Chem Phys*, 98 (1993) 5648.
17 Mohamed G G & Abd El-Wahab Z H, *Spectrochim Acta A,* 61 (2005) 1059.
18 Frisch M J, Trucks G W, Schlegel H B, Scuseria G E, Robb M A, Cheeseman J R, Montgomery J J A, Vreven T, Kudin K N, Burant J C, Millam J M, Iyengar S S, Tomasi J, Barone V, Mennucci B, Cossi M, Scalmani G, Rega N, Petersson G A, Nakatsuji H, Hada M, Ehara M, Toyota K, Fukuda R, Hasegawa J, Ishida M, Nakajima T, Honda Y, Kitao O, Nakai H, Klene M, Li X, Knox J E, Hratchian H P, Cross J B, Bakken V, Adamo C, Jaramillo J, Gomperts R, Stratmann R E, Yazyev O, Austin A J, Cammi R, Pomelli C, Ochterski J W, Ayala P Y, Morokuma K, Voth G A, Salvador P, Dannenberg J J, Zakrzewski V G, Dapprich S, Daniels A D, Strain M C, Farkas O, Malick D K, Rabuck A D, Raghavachari K, Foresman J B, Ortiz J V, Cui Q, Baboul A G, Clifford S, Cioslowski J, Stefanov B B, Liu G, Liashenko A, Piskorz P, Komaromi I, Martin R L, Fox D J, Keith T, Al-Laham M A, Peng C Y, Nanayakkara A, Challacombe M, Gill P M W, Johnson B, Chen W, Wong M W, Gonzalez C, & Pople J A, Gaussian, Inc., Gaussian 03, Revision C.02, Wallingford CT, (2004).
19 Dhanaraj C J, Hassan I U, Johnson J, Joseph J & Joseyphus R S, *J Photochem & Photobio B,* 162 (2016) 115.
20 Balakrishnan C, Subha L, Neelakantan M A & Mariappan S S, *Spectrochim Acta A,* 150 (2015) 671.
21 Narsimha N, Jaheer M, Reddy P R, Sudeepa K & Devi C S, *Indian J Chem*, 58A (2019) 436.
22 Bansod A D, Mahale R G & Aswar A S, *Russian J Inorg Chem,* 52 (2007) 879.
23 Abd El-Halim H, Mohamed G G & Anwar M N, *Appl Organometal Chem,* 32 (2018) e3899.
24 Elshaarawy R F M, Tadros H R Z, Abd El-Aal R M, Mustafa F H A, Soliman Y A & Hamed M A, *J Envir Chem Eng,* 4 (2016) 2754.
25 Mahmoud W H, Mahmoud N F, Mohamed G G, El-Sonbati A Z & El-Bindary A A, *J Mol Str,* 1095 (2015) 15.
26 Gupta S R, Mourya P, Singh M M & Singh V P, *J Organomet Chem*, 767 (2014) 136.
27 Yadav S & Singh R V, *Spectrochim Acta A,* 78 (2011) 298.
28 Shi Y C, Yang H M, Shen W B, Yan C G & Hu X Y, *Polyhedron,* 23 (2004) 15.
29 Gomosta S, Ramalakshmi R, Arivazhagan C, Haridas A, Raghavendra B, Maheswari K, Roisnel T & Ghosh S, *Z Anorg Allg Chem*, (2019) In Press.
30 Back D F, Oliveira G M, Canabarro C M & Iglesias B A, *Z Anorg Allg Chem,* 641 (2015) 941.
31 Banik B, Sarmah P P, Dutta A, Mondal P & Das P, *Indian J Chem*, 58A (2019) 29.
32 Bhanuka S & Singh H L, *Rasayan J Chem*, 10 (2017) 673.
33 Parsaee Z, *J Mol Str,* 1146 (2017) 644.
34 Annaraj B, Pan S, Neelakantan M A & Chattaraj P K, *Comput Theor Chem,* 1028 (2014) 19.
35 Kaur M, Jasinski J B, Anderson B J, Yathirajan H S & Byrappa K, *J Chem Crystallogr,* 46 (2016) 44.
36 Burlov A S, Vlasenko V J, Garnovskii D A, Polosareva N V, Antsyshkina A S, Sadikov G G, Sergienko V S, Churakov A V, Zubavichus Y V, Maltsev E I, Dmitriev A V, Lypenko D A, Cheprasov A S, Borodkin G S & Metelitsa A V, *Russian J Inorg Chem,* 59 (2014) 721.
37 Mahmoud W H, Mahmoud N F & Mohamed G G, *J Coord Chem,* 70 (2017) 3552.
38 Singh Y P, Patel R N & Singh Y, *Indian J Chem*, 57A (2018) 44.
39 Kahrovic E, Zahirovic A, Turkusic E & Bektas S, *Z Anorg Allg Chem*, 642 (2016) 480.
40 Belal A A M, El-Deen I M, Farid N Y, Zakaria R & Refat M S, *Spectrochim Acta A,* 149 (2015) 771.
41 Paswan S, Anjum A, Singh A P & Dubey R K, *Indian J Chem,* 58A (2019) 446.
42 Mahmoud W H, Deghadi R G & Mohamed G G, *Res Chem Intermed*, 42 (2016**)** 7869.
43 Sahoo J, Parween G, Sahoo S, Mekap S K, Sahoo S & Paidesetty S K, *Indian J Chem*, 55B (2016) 1267.
44 Abdel-Rahman L H, Abu-Dief A M, El-Khatib R M & Abdel-Fatah S M, *Bioorg Chem,* 69 (2016) 140.
45 Refat M S, Mohamed G G, de Farias R F, Powell A K, El-Garib M S, El-Korashy S A & Hussien M A, *J Therm Anal Calorim*, 102 (2010) 225.
46 Mahmoud W H, Mohamed G G & El-Sayed O Y, *Appl Organomet Chem*, 32(2) (2017) e4051.
47 Gulcan M, Ozdemir S, Dundar A, Ispir E & Kurtoglu M, *Z Anorg Allg Chem*, 640 (2014) 1754.
48 Suna Y X & Youb Z L, *Z Anorg Allg Chem*, 632 (2006) 1566.
49 Koçak N, Sahin M & Ucan H I, *Russian J Inorg Chem*, 57 (2012) 1227.
50 Raman N & Selvan A, *Russian J Inorg Chem*, 56 (2011**)** 759.
51 Garnovskii D A, Aleksandrov G G, Makarova N I, Levchenkov S I, Vlasenko V G, Zubavichus Y V, Uraev A I & Burlov A S, *Russian J Inorg Chem,* 62 (2017) 1077.
52 Khan M I, Khan A, Hussain I, Khan M A, Gul S, Iqbal M & Khuda I R F, *Inorg Chem Comm*, 35 (2013) 104.
53 Mahmoud W H, Mohamed G G & Mohamedin S Y A, *J Therm Anal Calorim*, 130 (2017) 2167.
54 Mahmoud W H, Mahmoud N F & Mohamed G G, *J Therm Anal Calorim*, 131(3) (2017) 2775.
55 You Z L & Zhu H L, *Z Anorg Allg Chem*, 632 (2006) 140.
56 Thangadurai T D & Natarajan K, *Indian J Chem,* 40 (2001) 573.
57 Chohan Z H, Pervez H, Rauf A, Khan K M & Supuran C T, *J Enzyme Inhib Med Chem,* 19 (2004) 417.
58 Gopalakrishnan S, Rajameena R & Vadivel E, *Int J Pharm Sci Drug Res,* 4 (2012) 31.
59 Tweedy B G, *Phytopathology,* 55 (1964) 910.
60 Abou-Hussein A & Linert W, *Spectrochim Acta A,* 141 (2015) 223.
61 Mahmoud W H, Deghadi R G & Mohamed G G, *J Therm Anal Calorim*, 127 (2017) 2149.
62 Mahmoud W H, Deghadi R G & Mohamed G G, *Appl Organomet Chem*, 30 (2016) 221.
63 Satheeshkumar R, Sayin K, Kaminsky W & Prasad K J R, *Monatsh Chem*, 149 (2018) 141.

64 Arafath M A, Adam F, Razali M R, Hassan L E A, Ahamed M B K & Majid A M S A, *J Mol Str*, 1130 (2017) 791.
65 Lakshmipraba J, Arunachalam S, Solomon R V & Venuvanalingam P, *J Coord Chem,* 68 (2015) 1374.
66 Akcha S, Hammal L, Triki S, Lezama L, Kolli B N & Baitich O B, *J Coord Chem,* 68 (2015) 4373.
67 Cheng Q R, Zhang F Q, Zhou H, Pan Z Q & Liao G Y, *J Coord Chem,* 68 (2015) 1997.
68 Ansari I A, Sama F, Shahid M, Ahmad M, Nayab P S, Rahisuddin & Siddiqi Z A, *J Coord Chem*, 69 (2016) 3336.
69 Mahmoud W H, Mohamed G G & Refat A M, *Appl Organomet Chem*, 31(11) (2017) e3753.